Epitaxial Ce and the magnetism of single-crystal Ce/Nd superlattices

P. S. Clegg*
Oxford Physics, Clarendon Laboratory, Parks Road, Oxford, OX1 3PU, United Kingdom

J. P. Goff
Department of Physics, University of Liverpool, Oliver Lodge Laboratory, Liverpool, L69 7ZE, United Kingdom

G. J. McIntyre
Institut Laue-Langevin, Boîte Postale 156, 38042 Grenoble Cedex 9, France

R. C. C. Ward and M. R. Wells
Oxford Physics, Clarendon Laboratory, Parks Road, Oxford, OX1 3PU, United Kingdom
(Received 18 October 2002; published 21 May 2003)

The chemical structure of epitaxial γ cerium and the chemical and magnetic structures of cerium/neodymium superlattices have been studied using x-ray and neutron diffraction techniques. The samples were grown using molecular-beam epitaxy, optimized to yield the desired Ce allotropes. The x-ray measurements show that, in the superlattices, both constituents adopt the dhcp structure and that the stacking sequence remains intact down to $T\sim 2$ K; these are the first measurements of magnetic ordering in single-crystal dhcp Ce. The magnetic structure of the superlattices with thicker Nd layers exhibit incommensurate order and ferromagnetism on separate sublattices in a similar manner to Nd under applied pressure. The sample with thickest Ce layers has a magnetic structure similar to bulk β Ce, which has commensurate transverse modulation with a propagation wave vector [1/2 0 0] and moments along the hexagonal *a* direction. These two types of magnetic order appear to be mutually exclusive. γ Ce is the high-temperature fcc phase of Ce, our single-phase epitaxial sample is observed to go through a new, but partial, structural transition not previously seen in the bulk material.

DOI: 10.1103/PhysRevB.67.174414 PACS number(s): 75.70.−i, 75.25.+z, 75.10.−b, 68.35.−p

I. INTRODUCTION

The electronic behavior of Ce has generated intense theoretical interest over several decades,[1] and the calculations of the structural[2] and magnetic[3] properties continue to yield new understanding. A range of structural phases exist because the energy of the inner $4f$ level is nearly the same as that of the valence $5d$ level. The allotropes have different atomic volumes and different nonintegral valencies. Here we study single-crystal Ce both as a thin film and as a constituent with Nd in superlattices of a range of compositions. We find that epitaxy has a profound effect on the structural phase transitions and that the magnetic interactions between Ce and Nd are very different to other light rare-earth superlattices.

When cooling bulk cerium from room temperature at atmospheric pressure three allotropes are encountered. Under ambient conditions, the stable phase is an fcc γ Ce. Below 275 K, there is an intermediate phase, dhcp β Ce, which is followed, at 110 K, by the collapsed phase, fcc α Ce. In practice, none of the structural phase transitions go to completion, and, at low temperatures, Ce samples tend to be a mixture of allotropes. The growth of single-phase β Ce is a difficult task; until now β Ce had been prepared from fcc γ Ce. The procedure involves taking single-crystal γ Ce and thermally cycling it for 10 or more times between room temperature and liquid-helium temperature. At this stage 90–95 % of the fcc γ Ce has converted into dhcp β Ce. The final few percents are converted by maintaining the sample at 348 K for one week. It is assumed that the γ-β transformation does not go to completion on cooling because it involves a slight expansion of the specific volume; heating the sample releases the compressive stresses on the remaining γ Ce and allows the transition to complete.[4] This technique can be used to prepare samples of better than 99% β Ce at room temperature. Upon cooling, a significant percentage of the β Ce will transform into fcc α Ce, so the sample will be a mixture of allotropes at low temperatures. This makes it impossible to characterize fully the phase with the dhcp crystal structure. The magnetic properties of the β Ce have been extrapolated from measurements on Ce_xY_{1-x} alloys;[5,6] it is assumed that β-Ce orders (below $T_N=12.7$ K) in an antiferromagnetic structure with moments lying in the basal plane on all sites in the unit cell. In this paper, the behavior of epitaxial γ Ce on cooling is studied and separately single-crystal dhcp β-Ce is successfully stabilized at low temperatures as part of Ce/Nd superlattices. The chemical and magnetic structures of Ce/Nd superlattices are studied across a range of compositions.

Nd is a dhcp light rare-earth metal. The dhcp light rare earths have two sublattices of sites with approximately hexagonal and cubic local symmetry which often show differing magnetic behavior creating an additional source of complexity. Below 19.9 K, Nd forms a longitudinally modulated magnetic structure involving moments on the hexagonal sites.[7] The moment is along the **a*** direction in the basal plane successive hexagonal planes order antiferromagnetically. Below 19.1 K, the moments tilt away from the **a*** direction to give a 2-q structure.[8] Further modulated struc-

tures occur below 10 K corresponding to the onset of order on the cubic sites. The 4-q magnetic structure is adopted at low temperature as a result of the coupling between the cubic and the hexagonal sites. Both the hexagonal and the cubic structures involve moments lying in the basal plane with the ordering being commensurate and incommensurate, respectively, for the two types of site.[9,8] In other Nd-based superlattices such as Pr/Nd (Ref. 10) and La/Nd (Ref. 11), the magnetic ordering is qualitatively similar to that of Nd metal.

Magnetic superlattices provide a unique way of probing the nature of exchange mechanisms in metals. To date most work on rare-earth superlattices has concerned hcp heavy rare-earth metals.[12–14] However, recently studies have been carried out on superlattices consisting of two light rare-earth metals.[15] Initial interest in heavy rare-earth superlattices was driven by the occurrence of long-range modulated magnetic structures, which propagated coherently through relatively thick nonmagnetic spacer layers. Subsequently, magnetic-magnetic superlattices were investigated and competition between the magnetic structures was observed. Of some relevance to the present work are the behaviors of Ho/Lu (Ref. 16) and Dy/Lu (Ref. 17) superlattices both of which exhibit transitions from helical magnetic structures to ferromagnetic states. Dy/Lu orders ferromagnetically with an elevated transition temperature while Ho/Lu forms a ferromagnetic phase at low temperature where none occurs in bulk Ho. It is generally assumed that this behavior is due to the compressive strain exerted by the Lu layers.

The first light rare-earth pair to be studied in a superlattice was Pr/Nd.[10] The constituents have similar melting points and lattice parameters simplifying the growth of a high-quality dhcp crystal structure. The magnetic structures of the series of samples studied range from bulk Nd behavior, including a temperature-dependent modulation wave vector and the complex 4-q low-temperature magnetic phase, to a simple magnetic structure in which just the hexagonal-symmetry sites ordered for thinner Nd layers. For a range of sample compositions order was induced on the hexagonal-symmetry sites in the Pr layers, and in one case a 2-q structure was observed. Additionally, La/Nd has been studied.[11] Samples of this combination proved to be very much harder to fabricate. Only two compositions could be grown successfully. Intriguingly, this system exhibited magnetic order on the hexagonal and cubic sites of the Nd layers and coexistent superconductivity, with a transition temperature close to that observed in bulk La.

The superlattice study presented in this paper concerns bilayers of Nd with Ce for which both the chemical and magnetic structures are of great interest. One of the possible consequences of introducing artificial periodicity into the chemical composition is that both constituents may be forced to adopt atypical lattice parameters. The amount of strain will alter with the superlattice composition and the resulting effect on the magnetic structure can be observed. There is also a possibility that the magnetic ordering may propagate through the intermediate layers, and there may be magnetic interactions between the two constituents of the superlattices.

Several previous attempts have been made to grow single-crystal single-allotrope superlattices incorporating Ce. A group of researchers tried to fabricate Ce/Ni multilayers[18] and it was found that the Ce immediately alloyed with the Ni even if the samples were grown and kept at liquid nitrogen temperatures. Another group grew Ce/Ta multilayers,[19] taking advantage of the immiscibility of these two elements. Ce layers of 15 Å and 5 Å were amorphous whereas those of 100 Å grew as fcc γ Ce but became a mixture of allotropes on cooling. Ce layers in Ce/Fe multilayers were amorphous for the thicknesses grown (10 Å to 60 Å).[20] It has been demonstrated that it is possible to improve the interface quality significantly by replacing Fe with FeCoV.[21] The work presented here demonstrates that single-crystal β Ce can be stabilized at low temperature.

Section II describes the growth of epitaxial Ce in thin films and as a superlattice constituent. Structural investigations with x rays are described in Sec. III; these show that both superlattice constituents adopt the dhcp structure while thin-film Ce has quite different behavior. Section IV details the neutron-scattering studies carried out on the Ce/Nd superlattices; these include the first measurements of magnetic ordering in single-crystal β Ce. The results are discussed in Sec. V.

II. SAMPLE GROWTH

The samples were grown using molecular-beam epitaxy onto 20×22 mm^2 sapphire substrates with an Nb buffer layer. The Ce film and the superlattices had significantly different requirements in terms of the choice of seed layer and growth conditions.

A. Epitaxial Ce film

The γ-Ce film was grown with a 500 Å layer of bcc Nb performing the function of both a buffer and a seed layer. The epitaxial relationships are (110) $Al_2O_3\|(110)$ Nb$\|(111)$ Ce. The Ce film was 5000 Å thick, and was evaporated at a rate of 0.5 Å s^{-1}. The substrate temperature was maintained at 673 K during growth and the Ce was protected from corrosion by a Nb cap. To investigate the stability of epitaxial Ce the crystal structure has been observed with x rays while a thermal cycling procedure was carried out.

B. Ce/Nd Superlattices

The Ce/Nd superlattices were grown using techniques similar to those employed previously for Pr/Nd superlattices.[22] It was found that good, single-phase β-Ce epitaxy could be established using a dhcp Pr seed layer on the Nb buffer. In this case, the epitaxial relationships are (110) $Al_2O_3\|(110)$ Nb$\|(001)$ Pr, Ce/Nd. This contrasts with evaporation directly onto bcc Nb which was successfully used to seed the growth of epitaxial γ Ce.

These Ce/Nd superlattices demonstrate that it is possible to grow dhcp β Ce as a single crystal in a layer of up to 30 planes. A series of compositions were grown and were subsequently studied at low temperature with neutrons. All com-

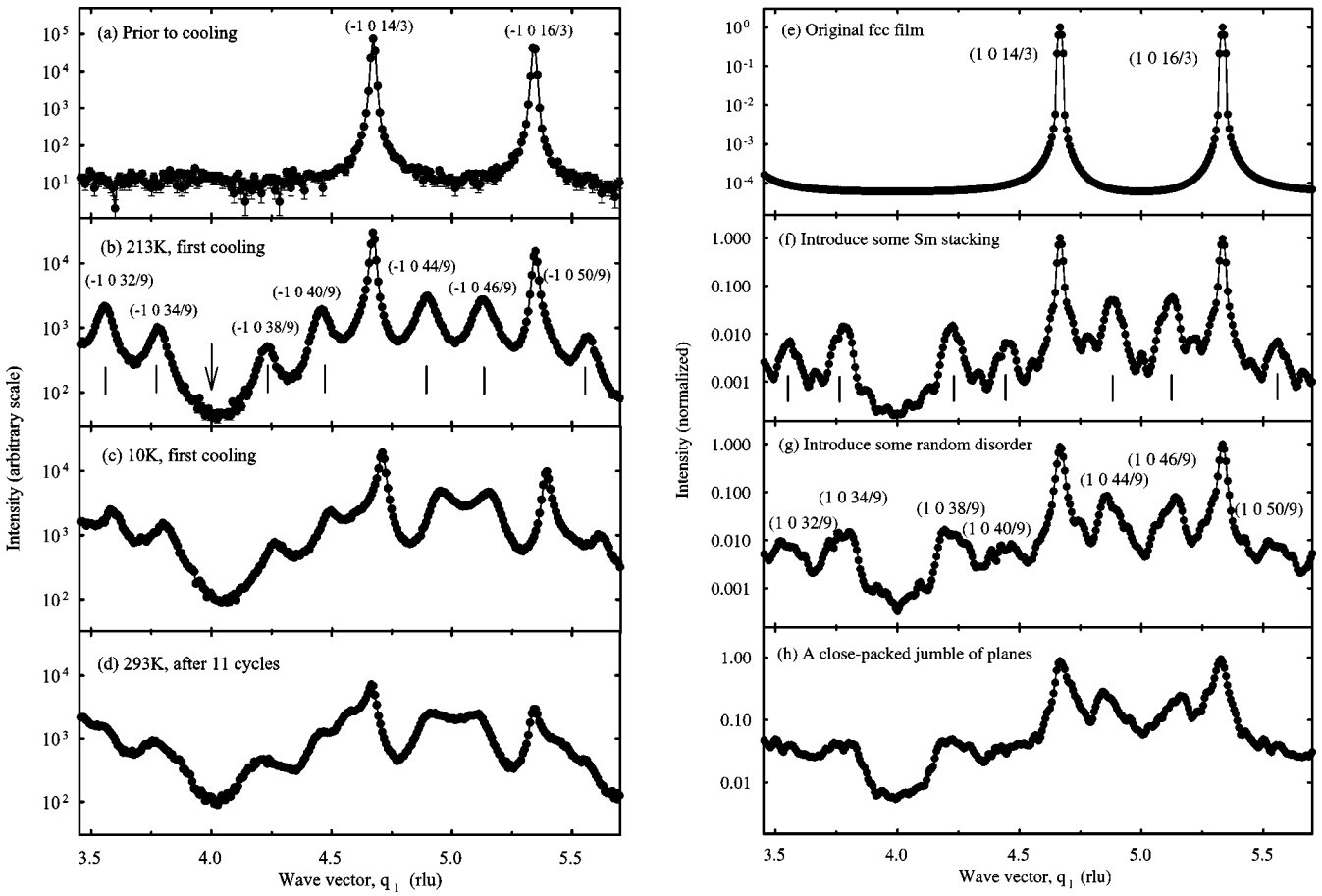

FIG. 1. (a-d) The x-ray scattering intensity measured in scans of **q** along $[\bar{1}\ 0\ q_l]$ for epitaxial γ Ce at various stages during thermal cycling: (a) original fcc sample, (b) cooled with additional Sm structure peaks marked by vertical bars, (c) at 10 K, and (d) after many cooling cycles. The arrow in (b) indicates one of the positions at which a peak would be expected for the dhcp packing sequence. (e)–(h) A simulation of the x-ray scattering intensity for epitaxial γ-Ce during the plane sliding transformation. The points (joined by lines) mark the wave-vector values for which the x-ray scattering has been simulated. Vertical bars mark the Sm structure peaks in (f). The Sm structure regions appear to become more numerous but smaller with thermal cycling.

positions of superlattice were grown on a 500-Å Nb buffer with a 1000-Å Pr seed layer and with both constituents being evaporated at 0.5 Å s^{-1}. The choice of substrate temperature is important for the growth of high-quality superlattices. With Pr/Nd[10] superlattices the constituents have similar melting temperatures. This facilitates finding a temperature at which good two-dimensional growth occurs without significant problems due to interdiffusion.[23] For the Ce/Nd system Ce has a considerably lower melting temperature than Nd, making the choice of substrate temperature more difficult. In addition, Ce is being forced to grow in a nonequilibrium structure by epitaxial constraint. The stability of the resulting structure is highly sensitive to changes in the substrate temperature. For Ce layers of up to 20 atomic planes a substrate temperature of 543 K gave good single-crystal β Ce, however, the growth of the sample with the thickest Ce layers posed a bigger challenge.

Growth of a superlattice with 30 atomic planes of Ce in each bilayer at 543 K still gave the dhcp crystal structure. Unfortunately, x-ray measurements showed that there was considerably more interdiffusion of the two constituents in this case than had been observed with the thinner Ce layers. Growth at much lower substrate temperatures creates a different problem. During fabrication, reflection high-energy electron diffraction (RHEED) scattering is measured. The RHEED pattern exhibits a change from streaks to spots, which indicates that the growth changes from two-dimensional planes to three-dimensional ''hillocks'' after a few planes have been deposited. The epitaxial strain forces the Ce planes to adopt particular lattice parameters. There is a buildup of coherency strain such that after the layer is just a few planes thick it becomes favorable to release the strain by a transition to three-dimensional growth. A balance was found at a substrate temperature of 453 K. The growth was two dimensional and the amount of interdiffusion was acceptable; the structural characteristics of the successfully grown samples are detailed in the following section.

III. STRUCTURAL ANALYSIS

The chemical structure at room temperature was determined by x-ray diffraction using high-resolution triple crystal diffractometers at the Clarendon Laboratory. Scans along $[1\ 0\ q_l]$ and $[0\ 0\ q_l]$ directions, in reciprocal space

were performed. (The hcp basis is used for labeling peaks throughout to provide a single notation for fcc-, dhcp-, and Sm-type crystal structures.) These scans give information about the quality of the film and the superlattices along the **c** direction, and enable the determination of the crystal structure. The widths of the (0 0 2) peaks obtained from scans along $[0\ 0\ q_l]$ could be used to deduce the real-space coherence length ξ of the spacing of close-packed planes in the growth direction since $\xi = 2\pi/\Delta q$, where Δq is the full-width at half maximum intensity (FWHM) in reciprocal space and the very high resolution of the x-ray diffractometer can be neglected. Scans of wave-vector transfer with q along $[1\ 0\ q_l]$ can be used to establish the stacking-sequence coherence length. Additionally, transverse scans through the (0 0 2) Bragg reflection were performed to measure the mosaic spread.

A. Epitaxial Ce film

A scan along $[\bar{1}\ 0\ q_l]$ is shown in Fig. 1(a). The positions of the peaks correspond to the fcc configuration of close-packed planes. The lattice parameter in the growth direction ($a = 5.167$ Å) corresponds to about the same value as the a lattice parameter observed in bulk γ Ce ($a = 5.161$ Å). The in-plane a lattice parameter ($a = 5.185$ Å) is considerably larger than that in bulk γ Ce, indicating that there is some distortion of the crystal structure. The Ce film was found to have a stacking-sequence coherence length of 300 Å and a mosaic spread of 0.26°. The coherence length is quite low, indicating a relatively high concentration of stacking faults.

Following measurements at room temperature the sample was mounted in a closed-cycle cryostat and was thermally cycled between room temperature and 10 K. Fig. 1(a)–(d) shows the x-ray scattering from scans along $[\bar{1}\ 0\ q_l]$ at various points in the thermal cycling procedure. It was found that the fcc γ-Ce to dhcp β-Ce phase transition does not occur in the epitaxial system. Instead, there is a transition at 245 K where some fraction of the sample transforms irreversibly into a structure with a nine-plane unit cell. The scattering observed from the new peaks [Fig. 1(b)] is consistent with that of the Sm-type crystal structure. The Sm-type structure is the nine-plane close-packed sequence[24] $\cdots ABABCBCAC \cdots$. The dhcp β-Ce structure would exhibit a peak in intensity at the position indicated by the arrow in Fig. 1(b). The coherence length corresponding to the Sm-type peaks is ~90 Å in comparison to ~200 Å from the $(\bar{1}\ 0\ q_l)$ fcc peaks at 213 K. There appeared to be no low-temperature transition equivalent to the transition to the collapsed phase of fcc α Ce which occurs in the bulk material. Instead, the Sm-type structure peaks are observed to broaden further. By analogy with the bulk γ-β transition, it was thought that thermal cycling might increase the yield of the Sm structure at the expense of the fcc structure. The experiment showed that the amount of fcc stacking decreased but that the close-packed planes became increasingly disordered. The plane-spacing coherence length determined from the (0 0 2) peak increased by only a few percent during the experiment while the mosaic spread remains constant, indicating that the significant changes in the stacking sequence were not affecting the crystalline quality.

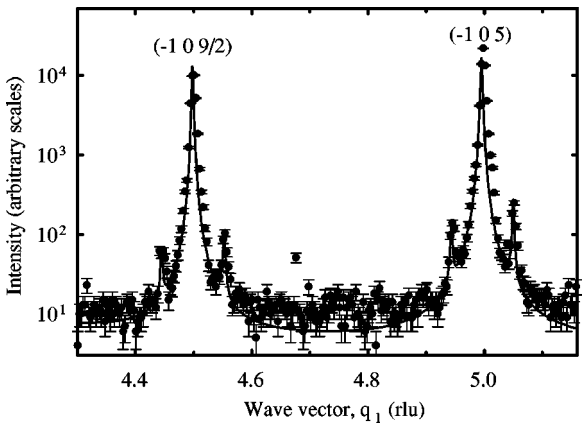

FIG. 2. The x-ray scattering observed for **q** along $[\bar{1}\ 0\ q_l]$ from $[Ce_{10}/Nd_{30}]_{70}$ showing the coherence of the dhcp stacking sequence over many bilayer repeats.

B. Ce/Nd superlattices

X-ray scattering measurements were obtained at room temperature for all the samples, nominally $[Ce_{10}/Nd_{30}]_{70}$, $[Ce_{20}/Nd_{20}]_{64}$, and $[Ce_{30}/Nd_{10}]_{60}$. Typically, coherence lengths $\xi \sim 1000$ Å were found. The FWHM of transverse scans through the main (0 0 2) Bragg peak for each sample give mosaic spread values in the range 0.15°–0.25°. These values are comparable with those measured for other rare-earth superlattices grown by MBE, and indicate that the samples are of good crystalline quality.

Figure 2 shows the x-ray scattering along $[\bar{1}\ 0\ q_l]$ for a superlattice sample and can be compared to that from fcc γ Ce in Fig. 1(a). This demonstrates that the Ce in the Ce/Nd superlattices adopts a dhcp structure uncontaminated by fcc Ce and this is one of the main results of the paper. For the sample with the thickest Ce layers, the reflections along the $[\bar{1}\ 0\ q_l]$ direction are slightly broader than those for the other samples indicating that there was a little more disorder in the sequence of stacking of the close-packed planes. The scans along the $[0\ 0\ q_l]$ direction reveal superlattice peaks at positions corresponding to the bilayer thickness (Fig. 3). To determine the strain and concentration profiles through the bilayer, these data are fitted to the structural model of Jehan *et al.*[25] The results (Table I) show that the lattice parameters of both the constituents are distorted compared to those of the bulk materials (bulk parameters $c_{Ce} = 2.964$; $a_{Ce} = 3.681$; $c_{Nd} = 2.949$; $a_{Nd} = 3.658$). The number of planes, λ, in the interface region (Table I) is slightly larger than that observed to date in rare-earth superlattices.

Neutron-scattering measurements were performed on the Ce/Nd superlattice samples as described in the following section. The dhcp structure was observed to remain intact down to $T \sim 2$ K, allowing magnetic measurements to be made on single-crystal β-Ce for the first time.

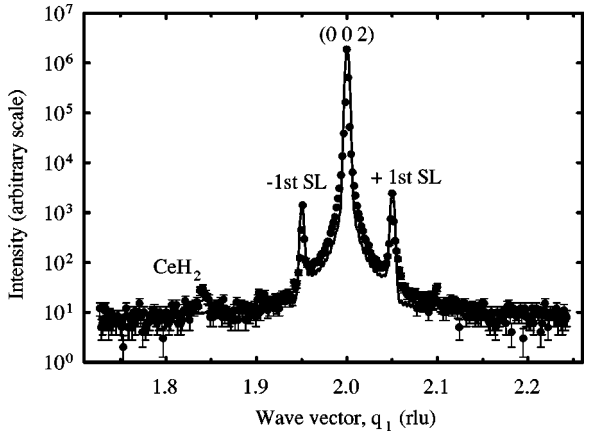

FIG. 3. Typical data for x-ray scans in the [0 0 q_l] direction for $[Ce_{20}Nd_{20}]_{64}$ through the (0 0 2) Bragg peak, showing superlattice peaks either side. The solid line shows a fit of a structural model to the data and is discussed in the text.

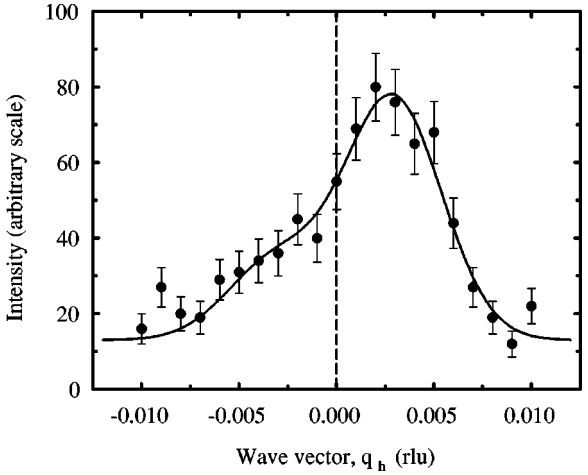

FIG. 4. Scan of **q** through the magnetic scattering at **q** ~(0 0.142 3/2) in a direction perpendicular to the magnetic modulation for $[Ce_{10}/Nd_{30}]_{70}$. The solid line is a fit to two Gaussian lineshapes with equal widths. The transverse splitting is a characteristic of the 2-q magnetic structure.

IV. MAGNETIC PROPERTIES OF Ce/Nd SUPERLATTICES

Neutron-diffraction measurements were carried out on the four-circle diffractometer D10 at the Institut Laue-Langevin. The superlattices were mounted in a variable-temperature helium-flow cryostat designed to fit within the Eulerian cradle.[26] Measurements of the magnetic structure were made between 2 K and 25 K. The incident energy was fixed at 14.8 meV and the higher-order contamination was suppressed using a pyrolytic graphite filter. The elastic magnetic signal from the superlattices is very weak, and it was necessary to suppress inelastic background using the optional energy-analyzer crystal. Unlike most other superlattices fabricated from pairs of rare-earth metals, the magnetic structure for Ce/Nd changes abruptly as the composition changes. The neutron-scattering results for each composition will be discussed separately.

A. $[Ce_{10}/Nd_{30}]_{70}$

A magnetic Bragg peak was observed at a wave vector **q**~(0.14 0 3/2) consistent with the simplest magnetic structure of bulk Nd, corresponding to incommensurate order on the hexagonal sites. The Néel temperature was 18 K, close to that of bulk Nd. Scans perpendicular to the ordering wave vector (0 0.14 3/2) at 2 K show signs of the formation of the 2-q magnetic structure (Fig. 4); otherwise, the wave vector was constant (q_h=0.14 rlu in the **a*** direction). The temperature dependence of the magnetic scattering integrated over both peaks is shown in Fig. 5(a). The integrated intensity of the magnetic scattering was observed to decrease slightly at the lowest temperatures. This decrease was subsequently confirmed by independent measurements on a second sample with the same composition. Scans in the **c*** direction (hexagonal **c** direction) through the antiferromagnetic order peak (Fig. 6), when corrected for the instrumental resolution, showed that the magnetic structure was coherent across about two bilayers and that this was independent of temperature. If there were no magnetic moment on the Ce sites, magnetic superlattice reflections would be observed on either side of the magnetic Bragg peak. The absence of superlattice peaks indicates that the same ordered structure has been induced on the Ce sites.

Ferromagnetism was detected via the temperature dependence of the $(\bar{1}\ 0\ 0)$ reflection [Fig. 7 and Fig. 5(b)] T_C =9 K. The magnetic structure factors were calculated using the expression

$$F_m = \left| \sum_j \mu_j e^{i\mathbf{q}\cdot\mathbf{r}_j} \right|, \tag{1}$$

where μ_j is μ_h for a hexagonal symmetry site and μ_c for a cubic symmetry site; the summation being over all sites in the unit cell. The structure factors were calculated for **q** values equal to various reciprocal lattice vectors (Table II). The magnetic structure factors for the (1 0 1/2)- and (1 0 3/2)-type positions depend only on the ferromagnetic component

TABLE I. Superlattice parameters determined using x-ray diffraction.

Sample	n_{Ce} ±2 planes	n_{Nd} ±2 planes	λ ±1 plane	c_{Ce} ±0.003 Å	c_{Nd} ±0.003 Å	a ±0.003 Å
$[Ce_{10}/Nd_{30}]_{70}$ A	12	28	6.5	2.973	2.942	3.626
$[Ce_{10}/Nd_{30}]_{70}$ B	10	28	6.5	2.965	2.944	3.652
$[Ce_{20}/Nd_{20}]_{64}$	21	19	6.5	2.962	2.947	3.656
$[Ce_{30}/Nd_{10}]_{60}$	24	10	5.5	2.970	2.949	3.664

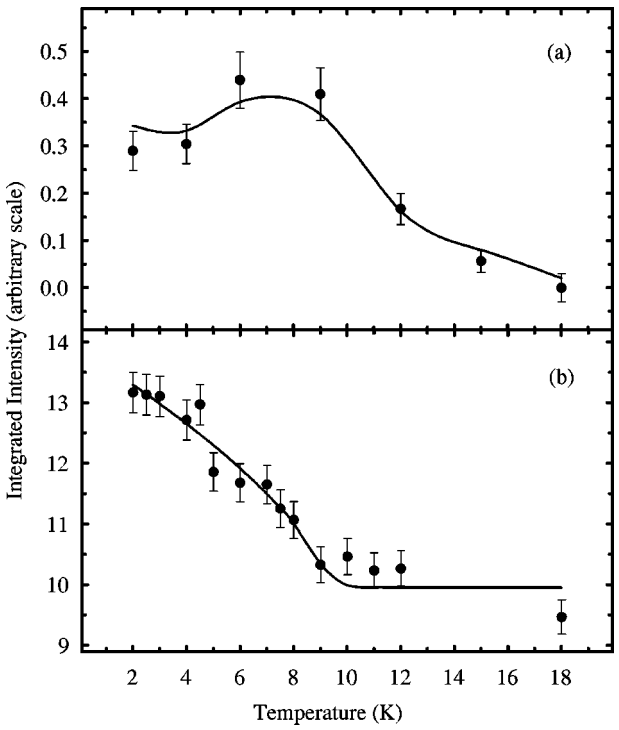

FIG. 5. Temperature dependence of the two magnetic structures in the $[Ce_{10}/Nd_{30}]_{70}$ samples (a) The integrated intensity at (0.14 0 3/2). (b) The intensity at the $(\bar{1}\ 0\ 0)$ due to ferromagnetic order. The solid lines are guides to the eye.

of the moment on the hexagonal sites μ_h. Measurements of the $(\bar{1}\ 0\ 3/2)$, $(\bar{1}\ 1\ 3/2)$, and (0 1 3/2) peaks at 2 K and 18 K are consistent with their being no ferromagnetic moment on the hexagonal sites $[\mu_h=(0.18\pm0.31)\ \mu_B]$. No magnetic scattering was observed at (0 0 1) indicating that the moments point along the **c** direction. The width of the peaks in the **c*** direction was comparable to that of the chemical-structure Bragg peaks, indicating that this magnetic structure was coherent throughout the superlattice. Such coherence throughout the sample suggests that the ferromagnetic moment exists on the cubic sites of both the constituents. A ferromagnetic *c*-axis moment occurs on the cubic sublattice in bulk Nd under applied pressure[27] making it likely that this behavior is driven by the Nd moments. The ferromagnetic intensity determined from the magnetic scattering at the $(\bar{1}\ 0\ 0)$ position at $T\sim2$ K would be consistent with a moment $\mu=(1.62\pm0.05)\ \mu_B$ on the Nd cubic sites, assuming that there is no moment on the Ce sites. The proposed magnetic structure in this superlattice is shown in Fig. 8. The moments on the hexagonal sites have a longitudinally modulated structure as with Nd just below the Néel temperature while the cubic-site moments are ferromagnetically aligned pointing along the **c** direction. Despite extensive searches, no magnetic scattering associated with the β-Ce magnetic structure nor the incommensurate Nd cubic-site order was detected down to a temperature $T\sim2$ K.

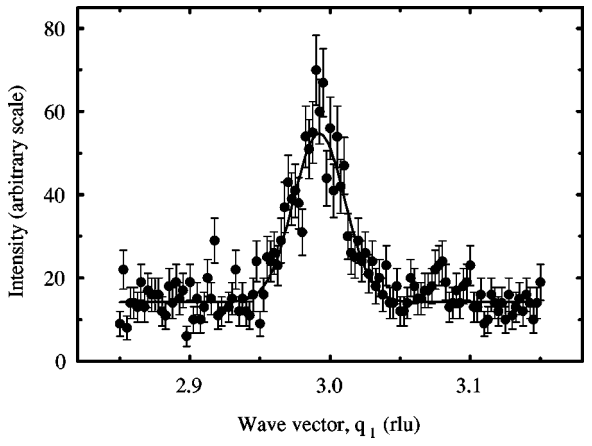

FIG. 6. Neutron-scattering intensity for $\mathbf{q}=(0.14\ 0\ q_l)$ for $[Ce_{10}/Nd_{30}]_{70}$ at 2 K. The width of the peak indicates that the magnetic structure is coherent approximately across two bilayers.

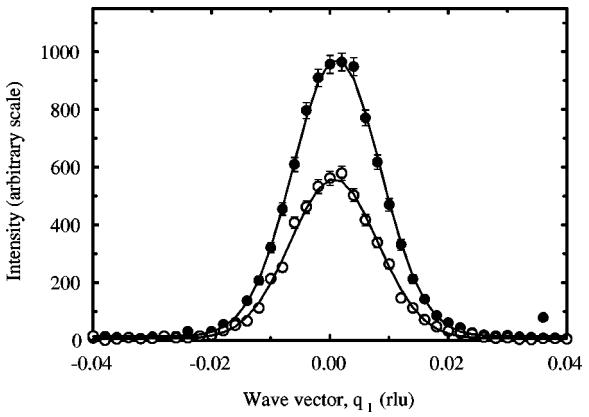

FIG. 7. Neutron-scattering intensity for $\mathbf{q}=(\bar{1}\ 0\ q_l)$ for $[Ce_{10}/Nd_{30}]_{70}$ at 2 K (full circles) and 18 K (open circles) showing ferromagnetic ordering.

B. $[Ce_{20}/Nd_{20}]_{64}$

The magnetic structures are qualitatively similar to $[Ce_{10}/Nd_{30}]_{70}$, however, there is a different domain population for the modulated structure. The 2-*q* incommensurate structure in Nd forms with 12 associated peaks representing $\pm q$ for the three possible domains as shown in Fig. 9(a). For this sample the neutron-scattering intensity was measured at the six peak positions shown in Fig. 9(b). Peaks were observed at the two positions which are shaded black which correspond to a single domain of the 2-*q* structure. Hence

TABLE II. Magnetic structure factors for dhcp ferromagnetic order.

q_h	q_k	q_l	$\lvert F(q)\rvert$
0	0	1	$2(\mu_c-\mu_h)$
0	0	2	$2(\mu_c+\mu_h)$
1	0	0	$2\ \mu_c-\mu_h$
1	0	$\frac{1}{2}$	$\sqrt{3}\ \mu_h$
1	0	1	$2\ \mu_c+\mu_h$
1	0	$\frac{3}{2}$	$\sqrt{3}\ \mu_h$

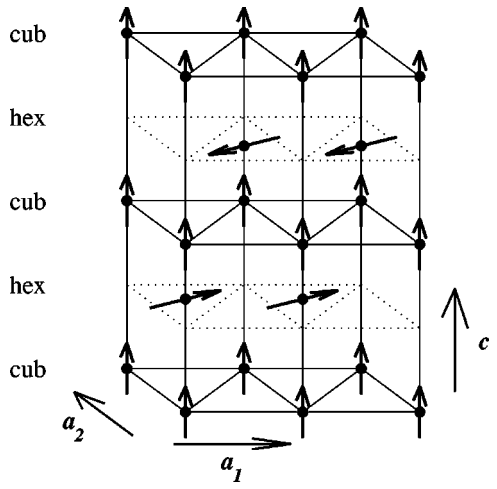

FIG. 8. The proposed magnetic structure in $[Ce_{10}/Nd_{30}]_{70}$. The superlattice $[Ce_{20}/Nd_{20}]_{64}$ has similar magnetic order. It is anticipated that the Nd magnetic moments drive the formation of this structure.

there is just a single domain of the incommensurate magnetic order at 2 K [Fig. 9(b)]. The total integrated intensity was 1/5 of that in the 30-plane Nd sample. c^* scans through a magnetic Bragg peak from this structure indicated that this order was only coherent within a single bilayer. These two features suggest that magnetic order is not induced on the Ce hexagonal sites for this sample. The *c*-axis ferromagnetic contribution was still very significant ($T_C = 10.5$ K) as witnessed by the temperature dependence of the (1 0 0) and (1 0 2) peaks and other peaks related by sixfold rotation. This magnetic structure was again restricted to the sites of cubic symmetry. The absence of superlattice reflections demonstrated that this structure existed throughout the bilayer. The scaling of the ferromagnetic moment with the thickness of the Nd layers supports the assumption that this magnetic structure is driven by the cubic sites of the Nd layers. Furthermore, this magnetic structure disappears altogether for the superlattice with the thinnest Nd layers. The integrated intensity of the ferromagnetic scattering at $T \sim 2$ K is consistent with $\mu = (1.55 \pm 0.14)\ \mu_B$ on the Nd cubic sites, the actual value being smaller than this due to the moment on the Ce cubic sites. Again the magnetic diffraction peaks of β Ce were not detected.

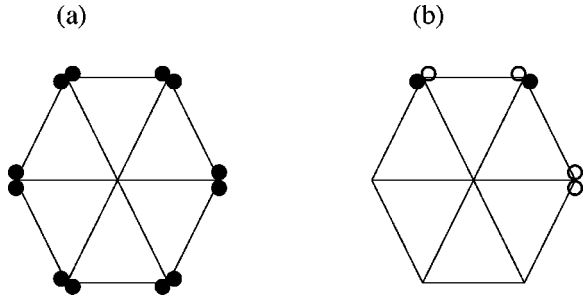

FIG. 9. (a) The peaks for the 2-*q* magnetic structure of an elemental Nd with all domains populated. (b) Scans were performed at these six points for $[Ce_{20}/Nd_{20}]_{64}$. Magnetic scattering was observed at the two positions that are shaded black. This corresponds to a single domain of the 2-*q* magnetic structure.

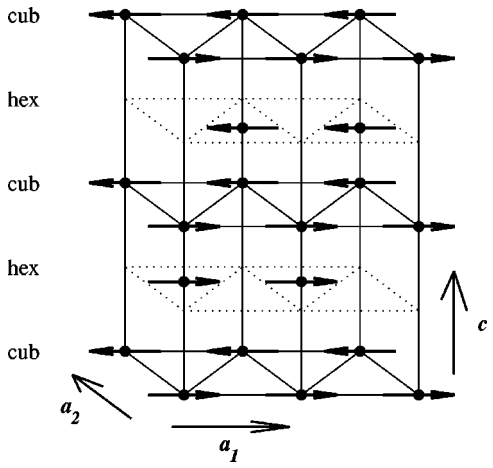

FIG. 10. The proposed β-Ce magnetic structure determined from measurements made on Ce_xY_{1-x} alloys[5,6] and found here for $[Ce_{30}/Nd_{10}]_{60}$.

C. $[Ce_{30}/Nd_{10}]_{60}$

For the sample with thickest Ce layers the magnetic order changed completely to being similar to that anticipated for β Ce (Fig. 10) from measurements made on Ce_xY_{1-x} alloys.[5,6] The strongest magnetic reflection at 2 K was observed at $(\overline{3/2}\ 0\ 0)$ (Fig. 11). The magnetic structure factors for the β-Ce structure (shown in Fig. 10) for the points in reciprocal space where magnetic scattering was observed are given in Table III. The relative strength of the scattering at $(\overline{1/2}\ 0\ 0)$ compared to $(\overline{3/2}\ 0\ 0)$ indicates that the magnetic ordering occurred on both cubic and hexagonal sites. When the Lorentz correction is included, the observed ratio of intensities was 6:1 whereas for the hexagonal sites to order alone a ratio of 4:1 would be anticipated while for cubic sites alone the ratio would be 1:1 (see Table III). The magnetic correlation lengths in the **c*** direction and in the basal plane are 54 Å and 580 Å, respectively. The **c*** correlation length was determined from magnetic scattering at the $(\overline{1/2}\ 0\ 3/2)$ position

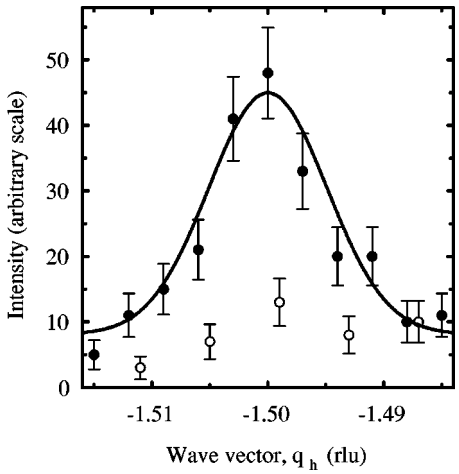

FIG. 11. Neutron-scattering intensity for $\mathbf{q} = (q_h\ 0\ 0)$ for $[Ce_{30}/Nd_{10}]_{60}$ at 2 K (full circles) and 18 K (open circles) showing ordering consistent with the β-Ce magnetic structure.

TABLE III. Magnetic structure factors for dhcp β-Ce order.

q_h	q_k	q_l	$\lvert F(q)\rvert$
$-\frac{1}{2}$	0	0	$4\ \mu_c - 2\ \mu_h$
$-\frac{1}{2}$	0	$\frac{1}{2}$	$-2\ \mu_h$
$-\frac{1}{2}$	0	1	$4\ \mu_c + 2\ \mu_h$
$-\frac{1}{2}$	0	$\frac{3}{2}$	$2\ \mu_h$
$-\frac{3}{2}$	0	0	$4\ \mu_c + 4\ \mu_h$
$-\frac{3}{2}$	0	1	$4\ \mu_c - 4\ \mu_h$
$-\frac{1}{2}$	1	1	$4\ \mu_c - 4\ \mu_h$

while the basal plane correlation length was found from the (3/2 0 0) peak. This choice was made to minimize the influence of the crystal mosaic spread on the measurement. The results indicate that the magnetic ordering is confined in single Ce blocks, and is possibly even shorter ranged than this. The moment on each Ce site is $\sim 0.1\mu_B$, somewhat smaller than measured in Ce_xY_{1-x} alloys.[5] Neither the hexagonal-site antiferromagnetic order nor the cubic site ferromagnetic order observed in the previous samples were detected in this sample. These magnetic structures appear to be mutually exclusive.

V. DISCUSSION

The experiments detailed above have revealed new structural behavior in a γ-Ce film and the complex magnetic phases of Ce/Nd superlattices.

A. Epitaxial Ce film

Epitaxial strain strongly modifies the structural phase transitions of γ Ce. The transformation from γ phase to β phase is completely suppressed in favor of a transformation from γ phase to a Sm-type crystal structure. The transition is partial, and on cooling below 120 K and with repeated thermal cycling the stacking sequence becomes disordered. For close-packed structures, the atomic volume does not have to change much for the different stacking sequences to become stable. In the bulk rare earths the changes between fcc $\rightarrow$dhcp$\rightarrow$Sm$\rightarrow$hcp transitions are believed to be associated with changes in the occupation of the $5d$ band.[27] Ce has the additional complication that intermediate-valence behavior is possible, and any electronic transitions are likely to be modified by epitaxial strain. Furthermore, the results indicate that the epitaxial film does not transform to a single equilibrium phase, but instead some degree of disorder is introduced.

The mechanisms for the γ-β and γ-Sm transitions can be compared. The mechanism for the γ-β phase transition is thought to be that two $\{0\ 0\ 1\}$ planes glide a distance a/6 while the next pair remains stationary.[4] The glide is equivalent to changing the letters of the stacking sequence cyclically:

fcc to dhcp transformation, four glides for nine planes

$$\begin{array}{ccccccccc} A & B & C & A & B & C & A & B & C \\ & & \Downarrow & & & & & & \\ A & B & A & B & C & A & B & C & A \\ & & & \Downarrow & & & & & \\ A & B & A & C & A & B & C & A & B \\ & & & & & & \Downarrow & & \\ A & B & A & C & A & B & A & B & C \\ & & & & & & & \Downarrow & \\ A & B & A & C & A & B & A & C & A. \end{array}$$

A transformation from fcc γ Ce to Sm structure requires that one plane slides while the next pair remains stationary. The full transition is observed to take fewer steps:

fcc to Sm transformation, three glides for nine planes

$$\begin{array}{ccccccccc} A & B & C & A & B & C & A & B & C \\ & & \Downarrow & & & & & & \\ A & B & A & B & C & A & B & C & A \\ & & & & & \Downarrow & & & \\ A & B & A & B & C & B & C & A & B \\ & & & & & & & & \Downarrow \\ A & B & A & B & C & B & C & A & C. \end{array}$$

The transformation favored by epitaxial strain involves less plane sliding without avoiding it altogether.

Figure 1(e)–(h) shows the results of a simulation of the epitaxial-plane-sliding phase transition. The simulation is similar to those used to study the hcp to fcc transition in Co and its alloys.[28,29] The model transformation was a effected in small domains picked at random within the 1350 planes of the film. A close-packed plane was coded by $p = 1(A), 2(B)$, or $3(C)$ and could be slid via

$$p' = (p \bmod 3) + 1, \tag{2}$$

where p' is the close-packed plane after it has slid: $p' = 2(B), 3(C)$, or $1(A)$, respectively. The size of the domains was chosen to follow the measured widths of the Sm structure peaks. Two processes were incorporated to capture the effect of thermal cycling. First, the domain size for the transformed regions was reduced. Second, random (but still close packed) disorder was introduced. The diffracted intensity was calculated by applying

$$I(q) = \left| \sum_j e^{i\mathbf{q}\cdot\mathbf{r}_j} \right|^2 \tag{3}$$

to the stack of close-packed planes for $\mathbf{q}$ values along $[10q_l]$; the summation is over all planes in the film. The simulated data was binned so that the resolution along q_l matched that of the instrument. The points (joined by lines) in Fig. 1(e)–(h) are the results of this simulation. The model results can be compared to the measurements in Fig. 1(a)–(d). The additional peaks in Fig. 1(f) are due to the domains ending unrealistically abruptly, a feature which disappears as

the amount of disorder increases. For the bulk transition from $\gamma \rightarrow \beta$ Ce, there is an increase in the specific volume which necessitates heating to drive the transformation to completion. It is likely that a similar small change in volume occurs in the epitaxial system and opposes the expansion of the Sm structure domains.

Perhaps unsurprisingly, this investigation demonstrates that the established thermal cycling technique is not an appropriate method for preparing epitaxial β-Ce samples.

B. Ce/Nd superlattices

The neutron-scattering experiments show a variety of magnetic structures that change with superlattice composition. The magnetic properties of the hexagonal sublattice in the 20- or 30-plane thick Nd layers has some similarities to the same sublattice in bulk Nd. Specifically, the moments are longitudinally modulated in the basal plane, as in bulk Nd, however, the ordering wave vector is independent of temperature. In complete contrast to bulk Nd at ambient pressure the cubic sublattice adopts a ferromagnetic alignment with the moment pointing along the *c* axis. For the sample with the thickest Ce layers, the coexistent ferromagnetic and antiferromagnetic order is no longer observed and the Ce adopts an antiferromagnetic structure with moments lying in the basal plane on both sublattices.

The behavior of samples with 20- or 30-plane thick Nd layers can be compared to the behavior of Nd under applied pressure. Experiments by Watson *et al*[30] show a sequence of changes to the magnetic structure with increasing pressure. For an applied pressure of 8.2 kbar the 4-*q* magnetic structure is suppressed and *c*-axis ferromagnetic ordering on the cubic sites is induced. As the pressure is increased to 11.6 kbar some domains of the antiferromagnetic structure are suppressed while the ferromagnetic, cubic-site moment gains a component in the basal plane. For the highest pressure applied (13.8 kbar), the ordering temperatures for the two structures became equal. Although not all of these features were observed in the measurements presented here, there are very strong similarities. Alloys of Nd with La,[31] Ce,[32] or Pr (Ref. 33) also exhibit coexistent ferromagnetic and antiferromagnetic order. In each case, the ferromagnetic moment is primarily associated with the cubic-symmetry sites while the incommensurate antiferromagnetic order is on the hexagonal sublattice. This behavior has been associated with the process of making Nd a *lighter* rare earth.[34] The epitaxial strain which Nd experiences in these Ce/Nd superlattices appears to have a similar effect to alloying or applied pressure. Strain-induced ferromagnetism in heavy rare-earth superlattices has been observed previously in Ho/Lu (Ref. 16) and Dy/Lu (Ref. 17).

The results also show that to understand the observed magnetic ordering it is important to consider the magnetic interactions between the two constituents of the superlattices. In the dhcp/dhcp superlattices Pr/Nd (Ref. 10) and La/Nd (Ref. 11) long-range magnetic ordering is observed, in contrast to hcp/dhcp Y/Nd (Ref. 35) where the magnetic order is found to be confined to individual Nd blocks. The propagation of magnetic order in superlattices is achieved via the establishment of conduction-electron spin-density waves in the spacer layers.[14,15] Whereas the matching of the Fermi surfaces in dhcp/dhcp superlattices allows the propagation of conduction electrons throughout the superlattice, the different crystal structures in hcp/dhcp superlattices result in their confinement to single blocks. Thus, coherence of the magnetic ordering is possible in dhcp/dhcp Ce/Nd superlattices.

There is some propagation of the antiferromagetic ordering of the Nd hexagonal sites through the Ce in the $[Ce_{10}/Nd_{30}]_{70}$ superlattice, but, in general, the antiferromagnetic Nd and Ce structures are of much shorter range than Pr/Nd and La/Nd. The difference for the Ce/Nd superlattices is that both constituents are magnetic at the temperatures studied, and there is a possibility of disruption of the propagation of the magnetic order due to the competition between the two different types of magnetic ordering. The magnetic structures of Nd and Pr are very similar at their ordering temperatures, indicating strong similarities in their Fermi surfaces. Thus Pr layers readily propagate the Nd magnetic order in Pr/Nd superlattices. In contrast, Ce and Nd exhibit very different magnetic structures, suggesting greater differences in their Fermi surfaces. The results indicate that the two types of antiferromagnetic structures cannot coexist in the same superlattice. A related phenomenon occurs in heavy rare-earth superlattices where, for example, the very different Ho and Er magnetic orderings become decoupled in Ho/Er superlattices.[36]

The dhcp Ce/Nd superlattices have two inequivalent sites, and like Pr/Nd and La/Nd the coupling of the Nd hexagonal sites differ from that of the cubic sites, presumably because different parts of the Fermi surfaces are responsible for the propagation of magnetic order. In fact, in some cases the Nd cubic sites exhibit ferromagnetic order that is coherent over many bilayer repeats so that the behavior is opposite to that of Pr/Nd and La/Nd. The coupling of ferromagnetic blocks across nonmagnetic spacer layers in rare-earth superlattices tends to be over a relatively shorter range.[37] It is possible that the long-range propagation of the ferromagnetic order in Ce/Nd superlattices is due to the inducement of the same ferromagnetic order on the Ce cubic sites. If this occurred at the Nd ordering temperatures, it would explain why Ce does not adopt its usual antiferromagnetic structure, which involves the cubic sites, at lower temperature.

The relationship between the ferromagnetic and incommensurate magnetic structures within the thicker Nd layers is unclear. The slight decrease at low temperatures, for the intensity of the incommensurate order peak [Fig. 5(a)], raises the possibility that the two structures are in competition. Additionally, it is a surprise that the incommensurate wave vector does not change as a function of temperature or at the onset of ferromagnetic order.

The growth of high-quality superlattices has facilitated magnetic measurements on a material with a highly unstable chemical structure. These results represent the first measurements on single-crystal β-Ce superlattices. The clamping affected by the superlattice suppresses the phase transition to the collapsed α-Ce phase on cooling. The sample with 30 atomic planes of Ce exhibited magnetic order of the type reported for dhcp Ce_xY_{1-x} alloys.[5,6] This is an antiferromag-

netic structure with moments lying in the basal plane on hexagonal and cubic sites. The wave vector $\mathbf{q}=(\frac{1}{2}\ 0\ 0)$ while moments point along (1 2 0). No magnetic ordering of this kind was detected in superlattices with thinner Ce layers, either due to interaction with the Nd or to epitaxial strain.

VI. CONCLUSIONS

Elemental dhcp β Ce has been successfully stabilized at low temperatures in the context of epitaxial Ce/Nd superlattices. The magnetic structures for the Ce/Nd superlattices change abruptly with changes of composition due to mutually exclusive magnetic ordering. The sample with the thickest Ce layers exhibits short-range order in an antiferromagnetic structure of the type anticipated for the bulk β Ce. The structural phase transitions of γ Ce have been observed to be strongly modified by epitaxy. A transformation from γ phase (fcc) to a Sm-type crystal structure was found in place of the transformation from fcc γ phase to dhcp β phase which occurs in the bulk material. In both cases, the pathological structural behavior of Ce has been modified via epitaxy.

ACKNOWLEDGMENTS

We would like to thank R.A. Cowley and R.S. Sarthour for useful discussions. Financial support was provided by the EPSRC in the UK and by the Institut Laue-Langevin in France. The expert technical assistance of the staff at the Institut Laue-Langevin is gratefully acknowledged.

*Present Address: Department of Physics, University of Toronto, Toronto, Ontario, Canada M5S 1A7.

[1] B. Johansson and M. S. S. Brooks, in *Handbook on the Physics and Chemistry of Rare Earths*, edited by K. A. Gschneider, Jr., L. Eyring, G. H. Lander, and G. R. Chopin (Elsevier, Amsterdam, 1993), Vol. 17, Chap. 112.

[2] K. Held, A.K. McMahan, and R.T. Scalettar, Phys. Rev. Lett. **87**, 276404 (2001).

[3] M.B. Zolfl, I.A. Nekrasov, T. Pruschke, V.I. Anisimov, and J. Keller, Phys. Rev. Lett. **87**, 276403 (2001).

[4] D. C. Koskenmaki and K. A. Gschneidner, Jr., in *Handbook on the Physics and Chemistry of Rare Earths*, edited by K. A. Gschneidner and L. Eyring (Elsevier, Amsterdam, 1978), Vol. 1, Chap. 4.

[5] E.P. Gibbons, E.M. Forgan, and K.A. McEwen, J. Phys. F: Met. Phys. **17**, L101 (1987).

[6] P.P. Deen, J.P. Goff, F. Yakhou, R.S. Sarthour, R.C.C. Ward, M.R. Wells, G.J. McIntyre, and D.F. McMorrow, J. Magn. Magn. Mater. **226**, 1145 (2001).

[7] R.M. Moon, W.C. Koehler, S.K. Sinha, C. Stassis, and G.R. Kline, Phys. Rev. Lett. **43**, 62 (1979).

[8] B. Lebech, J. Wolny, and R.M. Moon, J. Phys.: Condens. Matter **6**, 5201 (1994).

[9] E.M. Forgan, E.P. Gibbons, K.A. McEwen, and D. Fort, Phys. Rev. Lett. **62**, 470 (1989).

[10] J.P. Goff, C. Bryn-Jacobsen, D.F. McMorrow, R.C.C. Ward, and M.R. Wells, Phys. Rev. B **55**, 12 537 (1997).

[11] J.P. Goff, R.S. Sarthour, D.F. McMorrow, B.D. Rainford, C.J.T. Wilkins, R.C.C. Ward, and M.R. Wells, Physica B **241**, 714 (1998).

[12] C.F. Majkrzak, J. Kwo, M. Hong, Y. Yafet, D. Gibbs, C.L. Chien, and J. Bohr, Adv. Phys. **40**, 99 (1991).

[13] C. P. Flynn and M. B. Salamon, in *Handbook on the Physics and Chemistry of Rare Earths*, edited by K. A. Gschneider, Jr., and L. Eyring (Elsevier, Amsterdam, 1996), Vol. 26, Chap. 147.

[14] R.A. Cowley, J. Magn. Magn. Mater. **177**, 1156 (1998).

[15] J.P. Goff, R.S. Sarthour, D.F. McMorrow, F. Yakhou, A. Stunault, R.C.C. Ward, and M.R. Wells, Physica B **283**, 180 (2000).

[16] P.P. Swaddling, R.A. Cowley, R.C.C. Ward, M.R. Wells, and D.F. McMorrow, Phys. Rev. B **53**, 6488 (1996).

[17] R.S. Beach, J.A. Borchers, A. Matheny, R.W. Erwin, M.B. Salamon, B. Everitt, K. Pettit, J.J. Rhyne, and C.P. Flynn, Phys. Rev. Lett. **70**, 3502 (1993).

[18] C. Brouder, G. Krill, P. Guilmin, G. Marchal, E. Dartyge, A. Fontaine, and G. Tourillon, Phys. Rev. B **37**, 2433 (1988).

[19] Y. Aoki, H. Sato, Y. Komaba, Y. Kobayashi, H. Sugawara, S. Hashimoto, T. Yokoyama, and T. Hanyu, Phys. Rev. B **54**, 12 172 (1996).

[20] F. Klose, O. Schulte, F. Rose, W. Felsch, S. Pizzini, C. Giorgetti, F. Baudelet, E. Dartyge, G. Krill, and A. Fontaine, Phys. Rev. B **50**, 6174 (1994).

[21] S. Tixier, D. Mannix, P. Boni, W.G. Stirling, and G.H. Lander, Physica B **234**, 473 (1997).

[22] R.C.C. Ward, M.R. Wells, C. Bryn-Jacobsen, R.A. Cowley, J.P. Goff, D.F. McMorrow, and J.A. Simpson, Thin Solid Films **275**, 137 (1996).

[23] C.P. Flynn, J. Phys. F: Met. Phys. **18**, L195 (1988).

[24] W.C. Koehler and R.M. Moon, Phys. Rev. Lett. **29**, 1468 (1972).

[25] D.A. Jehan, D.F. McMorrow, R.A. Cowley, R.C.C. Ward, M.R. Wells, N. Hagmann, and K.N. Clausen, Phys. Rev. B **48**, 5594 (1993).

[26] C.M.E. Zeyen, R. Chagnon, F. Disdier, and H. Morin, Rev. Phys. Appl. **19**, 789 (1984).

[27] J.C. Duthie and D.G. Pettifor, Phys. Rev. Lett. **38**, 564 (1977).

[28] V.K. Kabra and Dhananjai Pandey, Acta Crystallogr., Sect. A: Found. Crystallogr. **51**, 329 (1995).

[29] S.P. Shrestha, V. Tripathi, V.K. Kabra, and Dhananjai Pandey, Acta Mater. **44**, 4937 (1996).

[30] D. Watson, E.M. Forgan, W.J. Nuttall, P.E. Sokol, S.J. Shaikh, S.W. Zochowski, and D. Fort, J. Phys.: Condens. Matter **8**, 5049 (1996).

[31] E.M. Forgan, S.L. Lee, W.G. Marshall, and S. Zochowski, J. Magn. Magn. Mater. **104**, 1519 (1992).

[32] E.P. Gibbons, E.M. Forgan, and K.A. McEwen, Physica B **156**, 774 (1989).

[33] K.A. McEwen, B. Lebech, and D. Fort, J. Magn. Magn. Mater. **54**, 457 (1986).

[34] E.M. Forgan, S.J. Shaikh, D. Fort, S. Zochowski, and C. Vettier, J. Magn. Magn. Mater. **104**, 1521 (1992).

[35] B.A. Everitt, M.B. Salamon, J.A. Borchers, R.W. Erwin, J.J.

Rhyne, B.J. Park, K.V. O'Donovan, D.F. McMorrow, and C.P. Flynn, Phys. Rev. B **56**, 5452 (1997).

[36] J.A. Simpson, D.F. McMorrow, R.A. Cowley, D.A. Jehan, R.C.C. Ward, M.R. Wells, and K.N. Clausen, Phys. Rev. Lett. **73**, 1162 (1994).

[37] J.P. Goff, R.S. Sarthour, C. Micheletti, S. Langridge, C.J.T. Wilkins, R.C.C. Ward, and M.R. Wells, J. Magn. Magn. Mater. **198**, 309 (1999).